ANALYSIS OF DEVELOPING LAMINAR FLOW AND HEAT TRANSFER IN A TUBE FOR A GAS WITH COOLING

by Alden F. Presler

Lewis Research Center
Cleveland, Ohio 44135

NATIONAL AERONAUTICS AND SPACE ADMINISTRATION • WASHINGTON, D. C. • FEBRUARY 1971

1. Report No.	2. Government Accession No.	3. Recipient's
NASA TN D-6152		

4. Title and Subtitle	5. Report Date
ANALYSIS OF DEVELOPING LAMINAR FLOW AND HEAT TRANSFER IN A TUBE FOR A GAS WITH COOLING	February 1971
	6. Performing Organization Code

7. Author(s)	8. Performing Organization Report No.
Alden F. Presler	E-5606
	10. Work Unit No.
9. Performing Organization Name and Address	129-01
Lewis Research Center National Aeronautics and Space Administration Cleveland, Ohio 44135	11. Contract or Grant No.
	13. Type of Report and Period Covered
12. Sponsoring Agency Name and Address	Technical Note
National Aeronautics and Space Administration Washington, D. C. 20546	14. Sponsoring Agency Code

15. Supplementary Notes

16. Abstract

Numerical solution of the boundary layer equations in the entire flow cross section for monatomic gases gives velocity and temperature profiles, Nusselt numbers, friction factors, and static pressures from the entrance region to nominal fully developed tube lengths. Moderate and high cooling fluxes are investigated. Larger fluxes produce adverse pressure gradients in the downstream tube sections which drastically modify the velocity and temperature profiles and the Nusselt and friction parameters. Rayleigh flow analysis predicts momentum pressure change within 25 percent of boundary layer calculations.

17. Key Words (Suggested by Author(s))	18. Distribution Statement
Friction factor; Gas flow; Pressure drop; Gas cooling; Laminar heat transfer; Cooling; Temperature profiles	Unclassified - unlimited

19. Security Classif. (of this report)	20. Security Classif. (of this page)	21. No. of Pages	22. Price*
Unclassified	Unclassified	39	$3.00

*For sale by the National Technical Information Service, Springfield, Virginia 22151

ANALYSIS OF DEVELOPING LAMINAR FLOW AND HEAT TRANSFER IN A TUBE FOR A GAS WITH COOLING

by Alden F. Presler

Lewis Research Center

SUMMARY

The compressible boundary layer equations are solved numerically for subsonic flow of a monatomic gas in a circular tube with uniform cooling flux on the walls. Initial fluid conditions are uniform, with velocity and temperature profiles developing downstream of the tube entrance.

Both moderate and high cooling flux conditions are investigated, including their effect on profiles, static pressure development, Nusselt numbers, and friction parameters based both on local shear stress and pressure drop.

Heat transfer and friction factor values for flows at moderate cooling approach those found in the constant property model. High cooling rates, however, distort the velocity profiles to such an extent (due to adverse pressure gradients) that Nusselt numbers and friction parameters deviate greatly from the standard constant property model.

Downstream of the entrance region, a very simplified calculation of the momentum pressure drop with Rayleigh flow assumptions gives values within 25 percent of the more exact boundary layer results in the case of the higher cooling flux.

INTRODUCTION

Reference 1 provided one of the earliest analyses of laminar flow with cooling which allowed temperature variation of the physical properties. The analysis of reference 1 was essentially fully developed in that the velocity and temperature profiles were independent of the axial coordinate. Heat transfer and friction parameters were obtained for both cooling and heating cases.

Reference 2 reported the numerical analysis of the compressible boundary layer equations for low subsonic gas flow with developing velocity and temperature profiles

and for both high heat flux input and essentially adiabatic conditions. Rather large deviations in fluid friction and heat transfer parameters compared with constant property results (ref. 5, chs. 9 and 13) were shown for cases of high heat flux.

The analytical portion of the present report has its basis in reference 2, and, in extending that into the problems of cooling heat transfer, it details the flow history of static pressure development and its momentum and frictional components.

This report contains a finite difference numerical analysis of the subsonic laminar flow of a compressible gas in a tube with uniform flux cooling heat transfer. Monatomic gas properties are used. The boundary layer equations are integrated across the tube radius without the use of the inviscid core assumption. The flow entering the tube is uniform in temperature and velocity, and these profiles develop with the flow through the tube. Effects of the level of cooling flux on local static pressure and velocity and temperature profiles are obtained, and from these basic variables are derived the variations in heat transfer and friction parameters. In this analysis all physical properties except specific heat have temperature dependency.

ANALYSIS

The steady-state momentum and energy boundary layer equations and the continuity equation, in axisymmetric cylindrical coordinates, are, respectively (ref. 5)

$$\rho u \frac{\partial u}{\partial z} + \rho v \frac{\partial u}{\partial r} = -\frac{dp}{dz} + \frac{1}{r} \frac{\partial}{\partial r} \left(r \mu \frac{\partial u}{\partial r} \right) \tag{1}$$

$$\rho C_p \left(u \frac{\partial t}{\partial z} + v \frac{\partial t}{\partial r} \right) - u \frac{dp}{dz} = \frac{1}{r} \frac{\partial}{\partial r} \left(rk \frac{\partial t}{\partial r} \right) + \mu \left(\frac{\partial u}{\partial r} \right)^2 \tag{2}$$

and

$$\frac{\partial \rho u}{\partial z} + \frac{1}{r} \frac{\partial \rho v r}{\partial r} = 0 \tag{3}$$

(Symbols are defined in the appendix.) The perfect gas law is

$$p = \rho \mathcal{R} t \tag{4}$$

The boundary and initial conditions for the system are

Initial $(z = 0,\ 0 \leq r \leq r_w)$:

$$u = u_i$$

$$v = 0$$

$$p = p_i$$

$$t = t_i$$

Centerline $(z > 0,\ r = 0)$:

$$u = u_o(z)$$

$$v = 0$$

$$t = t_o(z)$$

$$\frac{\partial u}{\partial r} = \frac{\partial t}{\partial r} = 0$$

Wall $(z > 0,\ r = r_w)$:

$$u = v = 0$$

$$+\left(k \frac{\partial t}{\partial r}\right)_w = q_w = \text{Constant}$$

The initial conditions are for uniform temperature and velocity profiles. The centerline conditions are results of the axial symmetry assumption. The wall conditions reflect the nonporous wall statement and the thermodynamic convention that heat added to the system is positive. Figure 1 is a model of this sytem, including initial and boundary conditions.

The system of equations (1) to (4) and the boundary conditions may be nondimensionalized by means of the following terms:

$$Z = \frac{\frac{z}{D}}{Re_i}$$

$$R = \frac{r}{r_w}$$

$$U = \frac{u}{u_i}$$

$$V = 2Re_i \frac{v}{u_i}$$

$$P^+ = \frac{p_i - p}{\rho_i u_i^2} = \frac{1 - \frac{p}{p_i}}{\gamma M_i^2}$$

$$T^+ = \frac{1 - \frac{t}{t_i}}{q^+}$$

$$\rho' = \frac{\rho}{\rho_i}$$

$$\mu' = \frac{\mu}{\mu_i}$$

$$K = \frac{k}{k_i}$$

$$C_p' = \frac{C_p}{C_{p,i}}$$

$$Re_i = \frac{\rho_i u_i D}{\mu_i} \qquad \text{(Reynolds number)}$$

$$Pr_i = \frac{C_{p,i} \mu_i}{k_i} \qquad \text{(Prandtl number)}$$

$$\frac{u_i^2}{C_{p,i}t_i} = (\gamma - 1)M_i^2 \qquad \text{(Eckert number)}$$

$$M = \frac{u}{a} \qquad \text{Mach number}$$

$$q^+ = \frac{q_w r_w}{k_i t_i}$$

The nondimensional system with boundary conditions is

$$\rho'\left(U\frac{\partial U}{\partial Z} + V\frac{\partial U}{\partial R}\right) = \frac{dP^+}{dZ} + \frac{4}{R}\frac{\partial}{\partial R}\left(R\mu'\frac{\partial U}{\partial R}\right) \tag{5}$$

$$\rho' C_p'\left(U\frac{\partial T^+}{\partial Z} + V\frac{\partial T^+}{\partial R}\right) - \frac{(\gamma - 1)M_i^2}{q^+}U\frac{dP^+}{Z} = \frac{4}{Pr_i}\frac{1}{R}\frac{\partial}{\partial R}\left(KR\frac{\partial T^+}{\partial R}\right) - \frac{4(\gamma - 1)M_i^2}{q^+}\mu'\left(\frac{\partial U}{\partial R}\right)^2 \tag{6}$$

$$\frac{\partial \rho' U}{\partial Z} + \frac{1}{R}\frac{\partial}{\partial R}(\rho' VR) = 0 \tag{7}$$

$$\rho' = \frac{1 - \gamma M_i^2 P^+}{1 - q^+ T^+} \tag{8}$$

Initial conditions ($Z = 0,\ 0 \leq R \leq 1$):

$$\left.\begin{aligned} U &= 1 \\ V &= 0 \\ P^+ &= 0 \\ T^+ &= 0 \end{aligned}\right\} \tag{9}$$

Centerline conditions ($Z > 0,\ R = 0$):

$$\left.\begin{aligned} U &= U_o \\ V &= 0 \\ T^+ &= T_o^+ \\ \frac{\partial U}{\partial R} &= \frac{\partial T^+}{\partial R} = 0 \end{aligned}\right\} \tag{10}$$

Wall conditions $(Z > 0,\ R = 1)$:

$$U = V = 0$$

$$-\left(\frac{\partial T^+}{\partial R}\right)_1 = \frac{1}{K_1} \tag{11}$$

$$K(Z, 1) = K_1$$

The radial velocity term for both energy and momentum equations is obtained in terms of the axial velocity from the continuity equation

$$\rho' V = -\frac{1}{R}\int_0^R R\,\frac{\partial \rho' U}{\partial Z}\,dR \tag{12}$$

$$\rho' V = -\frac{1}{R}\int_0^R R\left(\rho'\,\frac{\partial U}{\partial Z} + U\,\frac{\partial \rho'}{\partial Z}\right)dR \tag{13}$$

where

$$\frac{\partial \rho'}{\partial Z} = \frac{1}{1 - q^+T^+}\left(\rho' q^+ \frac{dT^+}{dZ} - \gamma M_i^2 \frac{dP^+}{dZ}\right) \tag{14}$$

The axial pressure gradient is obtained from the momentum equation at the wall $(R = 1,\ U = V = 0)$:

$$\frac{dP^+}{dZ} + 4\mu_1' \left.\frac{\partial^2 U}{\partial R^2}\right|_{R=1} + 4 \left.\frac{\partial U}{\partial R}\right|_{R=1} \left(\mu_1' + \frac{\partial \mu'}{\partial R}\right)_{R=1} = 0 \tag{15}$$

The thermal and transport properties are evaluated by the special relations

$$\left.\begin{aligned} \mu' = K = \left(\frac{t}{t_i}\right)^{0.68} &= (1 - q^+T^+)^{0.68} \\ C_p' &= 1 \\ Pr_i &= \frac{2}{3} \\ \text{and} \quad \gamma &= \frac{5}{3} \end{aligned}\right\} \tag{16}$$

These correspond closely to the properties of helium gas (ref. 2).

The radial derivatives of the transport properties are, for the preceding special relations,

$$\frac{\partial \mu'}{\partial R} = \frac{\partial K}{\partial R} = \frac{-0.68\, q^+}{(1 - q^+T^+)^{0.32}} \left(\frac{\partial T^+}{\partial R}\right) \tag{17}$$

which indicates that for vanishing heat flux we can assume constant property flow.

Numerical solution of the boundary layer system is accomplished by replacing the axial and radial derivatives by the finite difference approximations:

$$\frac{\partial U}{\partial Z} \cong \frac{\partial U}{\partial Z} = \frac{U_{j+1,k} - U_{j,k}}{\Delta Z} \tag{18}$$

$$\frac{\partial U}{\partial R} \cong \frac{\Delta U}{\Delta R} = \frac{U_{j,k+1} - U_{j,k-1}}{2\Delta R} \tag{19}$$

$$\frac{\partial^2 U}{\partial R^2} \cong \frac{\Delta}{\Delta R}\left(\frac{\Delta U}{\Delta R}\right) = \frac{U_{j,k+1} - 2U_{j,k} + U_{j,k-1}}{(\Delta R)^2} \tag{20}$$

where j, k are the axial and radial indices, respectively, of the finite difference mesh.

Friction and Heat Transfer Parameters

The local pressure and pressure gradient are calculated at each axial position, and the temperature and velocity profiles also as a function of radius. With these basic quantities, certain useful integral quantities can then be obtained.

$$U_b = 2\int_0^1 RUdR \tag{21}$$

$$T_b^+ = 2\int_0^1 R\rho' UT^+ dR \tag{22}$$

$$T_b = 2\int_0^1 R\rho' UT\, dR \tag{23}$$

where

$$T = T^+ - \frac{\gamma - 1}{2}\left(\frac{M_i^2}{q^+}\right)U^2 \tag{24}$$

$$Re_b = \frac{Re_i}{\mu_b'} \tag{25}$$

where

$$\mu_b' = (1 - q^+T_b^+)^{0.68} \tag{26}$$

$$Nu_b = \frac{2}{K_b(T_w^+ - T_b^+)} \tag{27}$$

where

$$K_b = \mu_b' = (1 - q^+T_b^+)^{0.68} \tag{28}$$

In terms of the dimensionless temperature ratio $\theta = (t - t_w)/(t_b - t_w)$, the bulk Nusselt number is

$$Nu_b = 2\left(\frac{\partial\theta}{\partial R}\right)_{R=1} \cdot \frac{k_w}{k_b} \tag{29}$$

Using the power relation for thermal conductivity,

$$Nu_b = 2\left(\frac{\partial\theta}{\partial R}\right)_{R=1} \cdot \left(\frac{t_w}{t_b}\right)^{0.68} \tag{30}$$

The friction factor based on the static pressure drop from the entrance to the axial distance z/D is defined as

$$f_{p,b} = \frac{\left(\frac{1}{2}\right)(p_i - p)}{\left(\frac{z}{D}\right)\rho_b u_b^2} \tag{31}$$

and in the dimensionless variables as

$$f_{p,b} = \frac{\frac{1}{2}P^+}{\left(\frac{z}{D}\right)U_b} \tag{32}$$

or

$$4f_{p,b}Re_b = \frac{2P^+}{U_b Z^+} \tag{33}$$

The friction factor based on the local shear stress is defined as

$$f_{\tau,b} = \frac{2\tau_w}{\rho_b u_b^2} \tag{34}$$

and the shear stress parameter of reference 1 is

$$\delta_b = \frac{\left(\frac{1}{2}\right)\tau_w D}{\mu_b u_b} \tag{35}$$

Then, from equation (34) and (35) we obtain

$$4f_{\tau,b}Re_b = \frac{8\tau_w D}{\mu_b u_b} \tag{36}$$

$$= 16\delta_b \tag{37}$$

The shear stress parameter is also written in dimensionless terms as

$$\delta_b = \frac{\tau_w'}{\mu_b' U_b} \tag{38}$$

where

$$\tau_w' = \frac{\tau_w r_w}{\mu_i u_i} \tag{39}$$

The numerical program provides values of P^+, U_b, $f_{\tau,b}$, and δ_b as functions of Z^+ and cooling flux q^+.

Momentum and Friction Pressure Drops

The decomposition of static pressure drop into friction and momentum components is readily followed through the impulse function of compressible gas dynamics (ref. 4, chs. 5, 8). The impulse function per unit area is

$$I = p + \rho_b u_b^2 \tag{40a}$$

$$= p + Gu_b \tag{40b}$$

where G is the mass flux. From the one-dimensional momentum equation

$$dI = dp + G\, du_b$$

$$= -4\tau_w\, d\left(\frac{z}{D}\right) \tag{41}$$

where τ_w is the local wall shear stress. Therefore, on integration of equation (41)

$$\Delta I = \Delta p + G\, \Delta u_b \tag{42a}$$

$$= -4\bar{\tau}_w\left(\frac{L}{D}\right) \tag{42b}$$

where L is the distance between measuring stations and $\bar{\tau}_w$ is the average shear stress.

Taking the lower limit of integration as the initial position or entrance to the tube, equation (42a) is

$$\Delta I = I - I_i \tag{43a}$$

$$\Delta I = (p - p_i) + G(u_b - u_i)$$

$$= -4\bar{\tau}_w\left(\frac{L}{D}\right) \tag{43b}$$

where u_b is the bulk velocity at the axial position Z units from the entrance.

Dividing both sides of equations (43) by $\rho_i u_i^2$ results in

$$\frac{\Delta I}{\rho_i u_i^2} = -\frac{4\bar{\tau}_w}{\rho_i u_i^2}\left(\frac{L}{D}\right) \tag{44a}$$

$$\frac{\Delta I}{\rho_i u_i^2} = -\frac{p_i - p}{\rho_i u_i^2} + \frac{G(u_b - u_i)}{\rho_i u_i^2} \tag{44b}$$

Since mass flux $G = \rho_b u_b = b_i u_i$, then equation (44) is written as

$$-\frac{4\bar{\tau}_w}{\rho_i u_i^2}\left(\frac{L}{D}\right) = -\frac{p_i - p}{\rho_i u_i^2} + \frac{\rho_b u_b}{p_i u_i}\left(\frac{u_b}{u_i} - 1\right)$$

$$= -P^+ + (U_b - 1) \tag{45}$$

Equation (45) states that the overall static pressure drop is the sum of the drop due to friction and the drop due to momentum change. Thus,

$$\Delta p_T = \Delta p_{FR} + \Delta p_M \tag{46}$$

Divide both sides of equation (46) by $\rho_i u_i^2$,

$$\frac{\Delta p_T}{\rho_i u_i^2} = \frac{\Delta p_{FR}}{\rho_i u_i^2} + \frac{\Delta p_M}{\rho_i u_i^2} \tag{47}$$

the left side of equation (47) is identifiable as the dimensionless pressure P^+. Hence, equation (47) is also written as

$$P^+ = P_{FR}^+ + P_M^+ \tag{48}$$

where

$$P_{FR}^+ = \frac{4\bar{\tau}_w}{\rho_i u_i^2}\left(\frac{z}{D}\right) \tag{49}$$

and

$$P_M^+ = (U_b - 1) \tag{50}$$

The numerical analysis provided values of P^+ and U_b as functions of z/D for each q^+ and M_i case. Equations (48) and (50) are used to compute the frictional P_{FR}^+ over the axial distance z/D for the one-dimensional compressible analysis.

Rayleigh Flow

Frictionless one-dimensional compressible tube flow with heat transfer (Rayleigh Flow) can be readily calculated for the uniform heat flux case. This simplified treatment provides a convenient way of comparing the idealized momentum change with the actual momentum change in a cooling situation.

The very complete and readable source for one-dimensional compressible flow theory in reference 4 is the background for this section and is taken from chapters 9 and 20 of that reference.

The energy balance for the tube with uniform heat flux and for the gas with constant specific heat is

$$T_2 = \frac{\dot{Q}}{C_p \dot{W}} + T_1 \tag{51}$$

where positions 1 and 2 are separated by tube distance z. Let us take position 1 as the initial point of flow and heating. The preceding equation is nondimensionalized with the initial temperature t_i,

$$\frac{T_2}{t_i} = \frac{\dot{Q}}{C_p t_i \dot{W}} + \frac{T_1}{t_i} \tag{52}$$

that is,

$$T' = 8q^+ \left(\frac{\frac{z}{D}}{Pe_i} \right) + T_i' \tag{53}$$

Again,

$$\frac{T'}{T_i'} = \frac{8q^+ \cdot Gz^{-1}}{T_i'} + 1 \tag{54}$$

which, for fixed M_i, t_i, and q^+, is a linear equation in the reciprocal Graetz variable. The temperature ratio in equation (54) is further nondimensionalized with the critical stagnation temperature T^* so that

$$\frac{\frac{T}{T^*}}{\frac{T_i}{T^*}} = \frac{8q^+ \cdot Gz^{-1}}{T_i'} + 1 \tag{55}$$

where for any Mach number

$$\frac{T}{T^*} = \frac{2(\gamma + 1)M^2\left[1 + \frac{\gamma - 1}{2} M^2\right]}{\left[1 + \gamma M^2\right]^2} \tag{56}$$

Again, for fixed M_i, t_i, and q^+ and for given values of Gz^{-1}, we calculate from equation (55) a succession of values of T/T^*. The Mach number M corresponding to this temperature ratio can be calculated from equation (56), or, more conveniently, from charts of T/T^* against M in reference 4.

The Mach number variation with heating (cooling) length is now the prime variable in calculating the static pressure development in the tube. Since impulse function is constant for frictionless flows,

$$p_2 + \left(\rho_b u_b^2\right)_2 = p_1 + \left(\rho_b u_b^2\right)_1 \tag{57a}$$

or

$$p_2\left(1 + \gamma M_2^2\right) = p_1\left(1 + \gamma M_1^2\right) \tag{57b}$$

Then,

$$\frac{p_2}{p_1} = \frac{1 + \gamma M_1^2}{1 + \gamma M_2^2} \tag{57c}$$

where Mach number is that of the local bulk velocity and sound velocity. If we identify p_1 and M_1 as belonging to the tube inlet,

$$P^+ = \frac{p_1}{\rho_1 u_1^2}\left(1 - \frac{p_2}{p_1}\right)$$

$$= \frac{1}{\gamma M_1^2}\left(1 - \frac{1 + \gamma M_1^2}{1 + \gamma M_2^2}\right)$$

$$= \frac{M_2^2 - M_i^2}{M_i^2\left(1 + \gamma M_2^2\right)} \tag{58}$$

A simplified treatment is possible for flows with low subsonic Mach numbers (say $M^2 < 0.1$). For this case equation (56) can be written as

$$\frac{T}{T^*} \cong 2(\gamma + 1)M^2 \tag{56a}$$

and therefore, equation (54) as

$$\frac{M^2}{M_i^2} \cong 1 + \left(\frac{8q^+}{T_i'}\right)Gz^{-1} \tag{54a}$$

Also, equation (58) is approximately

$$P^+ \cong \frac{M^2 - M_i^2}{M_i^2} = \frac{M^2}{M_i^2} - 1 \tag{58a}$$

Combining equations (54a) and (58a) gives us

$$P^+ \cong \left(\frac{8q^+}{T_i'}\right)Gz^{-1} \tag{59}$$

Equation (59) states that the dimensionless pressure drop for a frictionless gas flow, which is the same as the momentum pressure drop of equation (50), is directly proportional to the dimensionless flux and the dimensionless distance down the tube (inverse Graetz number), provided that $M^2 < 0.1$.

Equation (59) predicts an adverse pressure gradient in all sections of the tube for cooling in the absence of friction.

RESULTS AND DISCUSSION

The system of equations (5) to (11) were solved numerically for radial variations of U and T and for the axial variation of U, T, and P^+. These dependent variables were used in further calculation of the heat transfer (Nusselt) parameter and of the various and useful friction parameters. Calculations were carried out for combinations of values of the initial Mach number, M_i = 0.004, 0.06, and 0.30, and of the heat flux parameter, q^+ = -0.135, -1.35.

Velocity Profiles

Radial profiles of the axial velocity components for several axial positions, initial Mach numbers, and flux parameters, are shown in figure 2.

Development of the velocity profiles for the low heat flux cases (figs. 2(a) and (b)) follows closely that for laminar incompressible flow (ref. 5 - fig. 9.3, p. 231), becoming essentially a Poiseuille profile for distances of $Z^+ > 0.10$.

For the high cooling rate cases, the profiles for $Z^+ = 0.1$ reflect a cold dense gas along the wall which is decreasing in velocity under both adverse pressure gradient and density change, thus "thickening the boundary layer" and forcing more of the flow toward the centerline. The resulting centerline velocity excess in figures 2(c), (d), and (e) is opposite in behavior to the velocity profiles for gas cooling found in references 1 and 6 (fig. 9.16 therein). In reference 1 the radial velocity was omitted from the momentum equation, and the axial gradient $\partial u/\partial z$ was assumed to be small. These restrictions imposed a fully developed condition on the flow, under which the profile shape was determined by the temperature behavior of thermal conductivity and viscosity. Since gas viscosity decreased with cooling, shear stress decreased near the wall and velocity increased in that region thus decreasing the centerline velocity needed to maintain a given bulk velocity.

Temperature Profiles

Figures 3(a) and (b) for low heat flux conditions show that the temperature profile θ development in the axial direction is like that of the velocity profile. Values of θ for

$Z^+ \cong 0.1$ compare closely with fully developed values for $t_w/t_b = 1$ from reference 1 in which the flattening of the profiles is due to increased heat conduction in the wall region because of the lowering of gaseous thermal conductivity with decreasing wall temperature. In the present analysis for higher cooling flux the thickening boundary layer also convects cold fluid into the fas moving center stream. This augments the cooling because of the lower thermal conductivity near the wall, the effect of which on temperature profiles for $Z^+ \cong 0.1$ is seen in figures 3(c) to (e). These profiles are flatter than the fully developed case (fig. 3 of ref. 1).

Nusselt Numbers

Development of bulk Nusselt number with axial distance varies with the level of cooling heat flux. For initial Mach numbers of 0.004 and 0.06, figure 4(a) compares the values of Nu_b for $q^+ = -0.135$ and -1.35. The Nu_b for both cooling fluxes are similar to results of constant property analysis for $Gz^{-1} < 0.01$. However, downstream of that point the results for the higher cooling flux diverge from those of the lower flux and never reach a constant value that can be characterized as "fully developed" heat transfer, although figures 4(a) and (b) indicate for $q^+ = -1.35$ a somewhat sinusoidal variation in Nu_b around the value 7.0 ± 0.4 in the larger Gz^{-1} range.

On the other hand, the calculated Nu_b for the $q^+ = -0.135$ develop closely along the curve for constant property fluids with initially uniform conditions (ref. 2). This classical case asymptotically approaches the analytical value for the fully developed uniform heat flux case

$$\lim_{Gz^{-1} \to \infty} Nu = \frac{48}{11}$$

(ref. 5, p. 375).

The Nu_b increase for the $q^+ = -1.35$ value, as compared with the $q^+ = -0.135$ development, is attributed to the steeper temperature wall gradient. Recall the second expression for Nusselt number, equation (29),

$$Nu_b = 2\left(\frac{\partial \theta}{\partial R}\right)_{R=1} \cdot \left(\frac{k_w}{k_b}\right)$$

or

$$Nu_b = 2\left(\frac{\partial\theta}{\partial R}\right)_{R=1} \cdot \left(\frac{t_w}{t_b}\right)^{0.68}$$

The wall gradient $(\partial\theta/\partial R)_{R=1}$ increases quite rapidly in the region $0.01 \leq Gz^{-1} \leq 0.10$, while the temperature t_w/t_b decreases at a lower rate until $Gz^{-1} = 0.10$, where the absolute wall temperature has reached a value low enough to cause the temperature ratio to counteract the increasing temperature gradient. At this point the Nu_b reaches a maximum value of about 7.0 to 7.2. The decrease beyond the maximum Nusselt is caused by very low calculated wall temperatures. The numerical program was halted in this region of reciprocal Graetz numbers.

In reference 1, the influence of rate of heat flux on the fully developed Nusselt number was demonstrated by a correlation between Nu_b and the ratio t_w/t_b. By means of cross plotting data of the present numerical analysis, the developing Nusselt numbers were obtained as functions of the local t_w/t_b ratio. In the limit of fully developed heat transfer, the numerical Nu_b will approach the values of reference 1 as a limit. Figure 5(a) demonstrates that this does happen for the low heat flux case. Note that the data in figure 5(a) is divided into the entrance region of developing velocity and temperature profiles and the downstream region where velocity and temperatures are almost fully developed. Since there is no sharp separation point between these two regions, this division in figure 5(a) has arbitrarily been placed where our numerical Nusselt value is 110 percent of the fully developed Nusselt number of 48/11 for constant property analysis.

Two numerical runs for $q^+ = -1.35$, shown in figure 5(b) again demonstrate the marked effect of strong cooling on the boundary layer development and that effect, in turn, on derived variables such as Nusselt number. The reversal of the Nusselt number curve produces maximum values about 75 percent higher than the predictions from constant property analysis. Now up to $Z^+ \sim 0.01$ the similarity in development of velocity and temperature profiles for both $q^+ = -0.135$ and -1.35 (see figs. 2 and 3) is also observed in the developing Nusselt numbers (fig. 4). The developing flow region in figure 5(b) corresponds approximately to the same Z^+ as for that region in figure 5(a). There is, however, no quasi-developed flow region in figure 5(b) at the lower values of the temperature ratio t_w/t_b; there one finds instead the effects of rapidly increasing flow distortion due to the high cooling flux.

Friction Parameter and Pressure Drop

Friction factors based on wall shear stress are principally a function of the velocity profile gradient at the wall. The friction factor is defined by equation (34), and the

modified friction parameter $4f_{\tau,b}Re_b$ by equation (36).

Figures 6(a) and (b) give friction parameter results from the present analysis compared with Langhaar's linearized entrance region analysis (ref. 7) and the numerical boundary layer analysis for constant property fluids of reference 2. Figure 6(a) shows a very close similarity of development of the friction parameter between the present analyses for $q^+ = -0.135$ and the constant property calculations of reference 2.

With wall cooling fluxes of $q^+ = -1.35$, the velocity profiles with inflection points near the wall (figs. 2(c) to (e)) produce smaller wall shear stresses than for developing entrance flow of incompressible fluids. This in turn produces the lower friction parameters for the present numerical analysis which, in figure 6(b), are also compared with the calculations of references 2 and 7.

Reference 1 correlates the shear-stress parameter δ with the temperature ratio t_w/t_b to demonstrate the influence of heat flux rate on wall shear stress. As with the preceding discussion on the Nusselt number, the present numerical data for developing shear parameters was replotted to obtain the developing δ parameter correlated with t_w/t_b. The results compared with the fully developed predictions of reference 1 are presented in figure 7.

Both figures 7(a) and (b) have the similar entrance region development up to about $Z^+ \sim 0.01$ where velocity and temperature profiles approach fully developed values (figs. 2 and 3). This has been noted also in figures 5(a) and (b) for Nusselt numbers. Beyond $Z^+ \sim 0.01$ for the moderate $q^+ = -0.135$ there is quasi-developed flow, but the two almost identical curves for initial Mach numbers of 0.004 and 0.06 approach a limiting value of δ below the prediction of the fully developed analysis in reference 1. This divergence of shear results between boundary layer calculations and fully developed analysis, even for essentially incompressible flow, was first noted in reference 2. Heat flux, whether heating or cooling, and even at moderate values, has a more marked effect on friction characteristics of flow than it does on the heat transfer parameters.

At the higher cooling flux of $q^+ = -1.35$, the developing shear parameters δ plotted in figure 7(b) are similar to those in figure 7(a) to around $Z^+ \sim 0.01$. Downstream of that dimensionless length, the flow distortion due to cooling, which is discussed with reference to figures 2, 3, and 5(b), causes the shear stress to decrease rather rapidly with the lower values of the temperature ratio t_w/t_b.

The behavior of the static pressure drop for gas flow through the tube is always of practical interest, and the pressure drop for flow with uniform cooling at the walls is of additional interest because of the adverse effect on the flow due to the energy withdrawal. Figures 8 to 10 describe the effects of the cooling on the pressure or pressure related functions.

Figure 8 shows the average friction parameter $(4f_{pb}Re_b)$, based on the local static pressure drop from the entrance, as a function of the dimensionless distance Z^+. The

friction factor is given by equation (32), and the friction parameter actually plotted in figure 8 is given by equation (33). The friction factor (or parameter) is an averaged factor over the length Z^+.

Figure 8(a) compares the present numerical results for moderate cooling and $M_i = 0.004$ and 0.06 with results of constant property fluids from boundary layer analysis (ref. 2), a linearized entrance region analysis (ref. 7), and the classical fully developed Poiseuille case. The present results are essentially the same as the earlier numerical results.

The friction parameters for the higher cooling rate case at $M_i = 0.004$, 0.06, and 0.30 are plotted on figure 8(b). Comparison is again made with the adiabatic incompressible numerical results of reference 2 and the linearized entrance analysis of reference 7. In addition, friction parameters shown in figure 8(b) extending from $Z^+ = 0.0001$, have a curve closely fitting the experimental data of reference 8, which was for adiabatic incompressible laminar boundary layers in the entrance region of a tube up to $Z^+ = 0.001$. The strong downward turn of the curves for the present numerical results starts around $Z^+ = 0.01$, which coincides with the similar behavior of the curves in figure 7(b) for wall shear stress and indicates the relation between the two variables. In the present calculations for higher cooling flux, the static pressure did rise above the initial p_i, which resulted in negative friction parameters. Since these could not be shown on the logarithmic plots of figure 8, this behavior will be discussed on the next figure.

The development of dimensionless static and frictional pressure drops are recorded in figure 9. The dimensionless static pressure P^+ was calculated directly in the numerical program. The pressure drop from momentum change in the flow, is related to the bulk velocity by equation (50) and the pressure drop due to frictional effects is the difference between these two, as is given by equation (48).

In figures 9(a) and (b) the pressure plots for $M_i = 0.004$ and 0.06 at the moderate $q^+ = -0.135$ indicate a small positive momentum pressure due to the developing velocity profile in the entrance region of the tube. The cooling soon reverses the sign on the momentum pressure so that the static pressure is less than the friction pressure for the rest of the tube length. The momentum pressure is not a significant part of the overall static pressure in the moderate cooling cases, and it is seen that the friction pressure and static pressure are virtually the same over most of the tube length.

The pressure drops in the higher cooling level are shown in figures 9(c) to (e). The static pressure is seen to reach a maximum in the vicinity of $Z^+ = 0.01$ and decreases steadily from that region. The difference between the friction pressure and the static pressure shown is the negative momentum pressure. It is interesting that the friction pressure for $Z^+ > 0.015$ increases very slowly compared with its earlier behavior. Since the pressure values are cumulative along the tube, this almost constant value of

friction pressure indicates a sharp decrease in wall friction, which we have already observed in figure 7.

These variations in the dimensionless pressure P^+ indicate a rise in static pressure and a thickening of the wall boundary layer in the downstream tube sections at the higher cooling flux. This adverse pressure gradient recalls a similar situation in external flows where thickening of the boundary layer precedes separation. In the present case of internal flows, the static pressure rise is accompanied by a continual decrease in the bulk velocity and persistance of flow in face of static pressure increase is due to the fluid inertia.

Rayleigh Flow Calculations

The shear stress friction factors of figures 6 and 7 show that the standard incompressible or fully developed correlations do not describe the frictional behavior of highly cooled gas flows, but they do describe the development of the moderate cooling cases. We can inquire whether the momentum "friction" or pressure can be predicted by use of the Rayleigh calculations for one-dimensional frictionless heat transfer. These Rayleigh calculations have been carried out and are compared in figure 10 with the momentum pressure drop calculated from the present numerical boundary layer analysis.

The results of the momentum calculations for the moderate cooling levels for $M_i = 0.004$ and 0.06 are given in figure 10(a). Rayleigh momentum pressures with cooling are always negative from the tube entrance. The boundary layer momentum pressure, even with cooling, is slightly positive close to the entrance because of the establishment of the velocity profile. The general shapes of the curve pairs are similar.

Logarithmic plots of Rayleigh flow - boundary layer flow momentum pressures for the higher cooling fluxes are given in figures 10(b) to (d). The nature of the logarithmic scale accentuates the discrepancy between the two results at the lower values of the Z^+. In terms of the absolute values, the Rayleigh and boundary layer results do not differ greatly. At the limit of the Z^+ range the difference is 10 to 20 percent.

The interesting point with these calculations at $q^+ = -1.35$ is that the Rayleigh flow results underpredict the momentum pressure for the larger ranges of Z^+. This is again due to the change in the velocity profiles in these Z^+ ranges. Profiles that are deviating from fully developed contours have a positive momentum pressure component which opposes the negative component arising from the bulk velocity decrease.

SUMMARY OF RESULTS

The compressible momentum and energy boundary layer equations are numerically solved for subsonic flow of a monatomic gas in a circular tube with initial uniform velocity and temperature profiles (at $Z^+ = 0$), and with uniform wall cooling at flux levels q^+ of -0.135 and -1.35. The results of the calculations are as follows:

1. At the lower cooling flux, the axial development of velocity and temperature profiles, friction factors and Nusselt numbers, closely follow classical results for constant property fluids.

2. For the higher cooling flux cases, the more important results are:

a. In the downstream tube section, the velocity profiles thicken and the flow is similar to that of unconfined flows approaching a separation point.

b. The increasing transverse velocity accompanying the thickening boundary layer augments thermal convection and flattens the radial temperature profiles.

c. The bulk Nusselt number rises to a value 75 percent greater than the fully developed value of 48/11 for constant property fluids.

d. Decreasing wall shear depresses the local friction factor values to less than one-half the Poiseuille limit.

e. Static pressure increases above ambient as the fluid slows down under cooling, and adverse pressure gradients occur in conjunction with the thickening boundary layer.

f. Rayleigh flow analysis gives momentum pressure drops within 25 percent of those obtained from the numerical boundary layer solution.

Lewis Research Center,
National Aeronautics and Space Administration,
Cleveland, Ohio, October 16, 1970,
129-01.

APPENDIX - SYMBOLS

a	local sound velocity, $\sqrt{\gamma \mathscr{R} t}$
C_p	heat capacity at constant pressure
D	diameter of tube
$f_{p,b}$	friction factor based on pressure drop with density evaluated at bulk temperature, $(+1/2)\,(p_i - p) \Big/ \left[(z/D)\rho_b u_b^2\right]$
$f_{\tau,b}$	friction factor based on local wall shear stress with properties evaluated at bulk temperature, $\tau_w \Big/ (1/2)\rho_b u_b^2$
G	mass flux
Gz	Graetz number, $Pe \Big/ (z/D)$
h	local heat transfer coefficient, $q_w \Big/ (t_w - t_b)$
K	dimensionless thermal conductivity, $k \Big/ k_i$
k	gas thermal conductivity
M	local Mach number, u/a
Nu_b	local bulk Nusselt number, hD/k_b
P^+	dimensionless pressure drop, $(p_i - p) \Big/ \rho_i u_i^2$
Pe	Peclet number, $Pr_i Re_b$
P_{FR}^+	dimensionless pressure drop due to friction, eq. (49)
P_M^+	dimensionless pressure drop due to momentum, eq. (50)
Pr_i	initial Prandtl number, $C_p u_i \Big/ k_i$
p	static pressure
p'	local static pressure ratio, p/p_i
$\dot{Q}$	cooling rate, energy per unit time
q_w	cooling flux at wall, energy per unit time per unit wall area
q^+	dimensionless cooling flux parameter, $q_w r_w \Big/ k_i t_i$
R	dimensionless radius, r/r_w
$\mathscr{R}$	gas constant
Re_b	bulk Reynolds number, $Du_b\rho_b \Big/ \mu_b$
Re_i	initial Reynolds number, $Du_i\rho_i \Big/ \mu_i$

r	radial distance
r_w	tube radius
T	dimensionless total temperature, $T^+ - 1/2\left[(\gamma - 1)/q^+\right]M_i^2U^2$
T^+	dimensionless static temperature, $(1 - t')/q^+$
t	static temperature
t'	local static temperature ratio, t/t_i
U	dimensionless axial velocity, u/u_i
u	axial velocity component
V	dimensionless radial velocity, $2(v/u_i)Re_i$
v	radial velocity component
$\dot{W}$	flow rate, mass per unit time
Z	dimensionless axial distance, $(z/D)/Re_i$
Z^+	modified axial distance, $(z/D)/Re_b$
z	distance along tube from entrance
γ	ratio of specific heats, C_p/C_v
δ_b	shear stress parameter, based on bulk properties, $\tau_w r_w/\mu_b u_b$
θ	static temperature ratio, $(t - t_w)/(t_b - t_w)$
μ	gas viscosity
μ'	dimensionless viscosity, μ/μ_i
ρ	gas density
τ_w	local wall shear stress
$\bar{\tau}_w$	average wall shear stress over tube length z

Subscripts:

b	bulk average at local axial position
i	initial ($Z = 0$) condition
j, k	mesh positions in difference technique
o	centerline ($r = 0$) conditions
w	tube wall conditions

REFERENCES

1. Deissler, Robert G.: Analytical Investigation of Fully Developed Laminar Flow in Tubes with Heat Transfer with Fluid Properties Variable Along the Radius. NACA TN 2410, 1951.

2. Deissler, Robert G.; and Presler, Alden F.: Analysis of Developing Laminar Flow and Heat Transfer in a Tube for a Gas with Variable Properties. Proceedings of the Third International Heat Transfer Conference. Vol. 1. AIChE, 1966, pp. 250-256.

3. Hughes, W. F.; and Gaylord, E. W.: Basic Equations of Engineering Science. Schaum Publishing Co., 1964, pp. 29, 36, 37.

4. Kunkle, John S.; Wilson, Samuel D.; Cota, Richard A., eds.: Compressed Gas Handbook. NASA SP-3045, 1969.

5. Knudsen, James G.; and Katz, Donald L.: Fluid Dynamics and Heat Transfer. McGraw-Hill Book Co., Inc., 1958.

6. McAdams, William H.: Heat Transmission. Third ed., McGraw-Hill Book Co., Inc., 1954.

7. Langhaar, Henry L.: Steady Flow in the Transition Length of a Straight Tube. J. Appl. Mech., vol. 9, no. 2, June 1942, pp. 55-58.

8. Shapiro, A. H.; Siegel, R.; and Kline, S. J.: Friction Factor in the Laminar Entry Region of a Smooth Tube. Proceedings of the Second U. S. National Congress of Applied Mechanics, Paul M. Naghdi, ed., ASME, 1955, pp. 733-741.

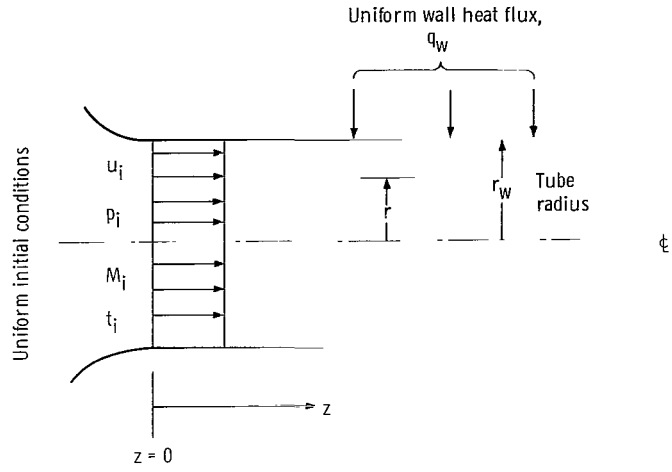

Figure 1. - Flow geometry with initial conditions.

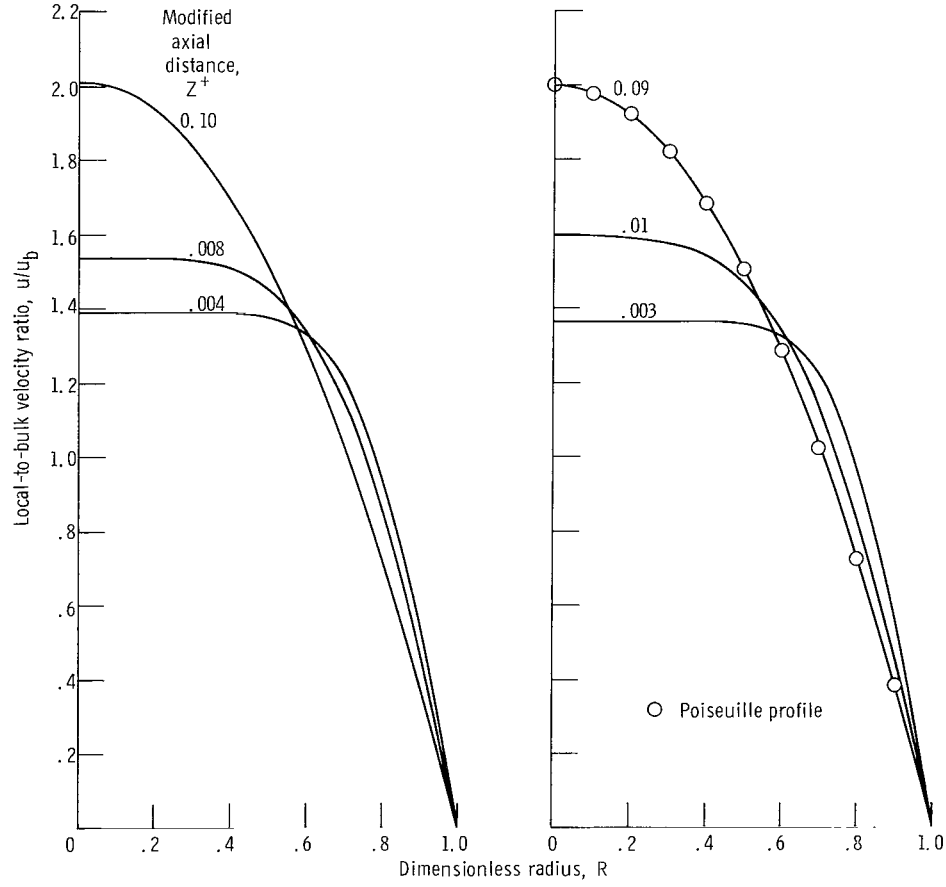

(a) Initial Mach number, 0.004; dimensionless cooling flux parameter, -0.135 (low cooling flux).

(b) Initial Mach number, 0.06; dimensionless cooling flux parameter, -0.135 (low cooling flux).

Figure 2. - Developing velocity profiles across tube radius.

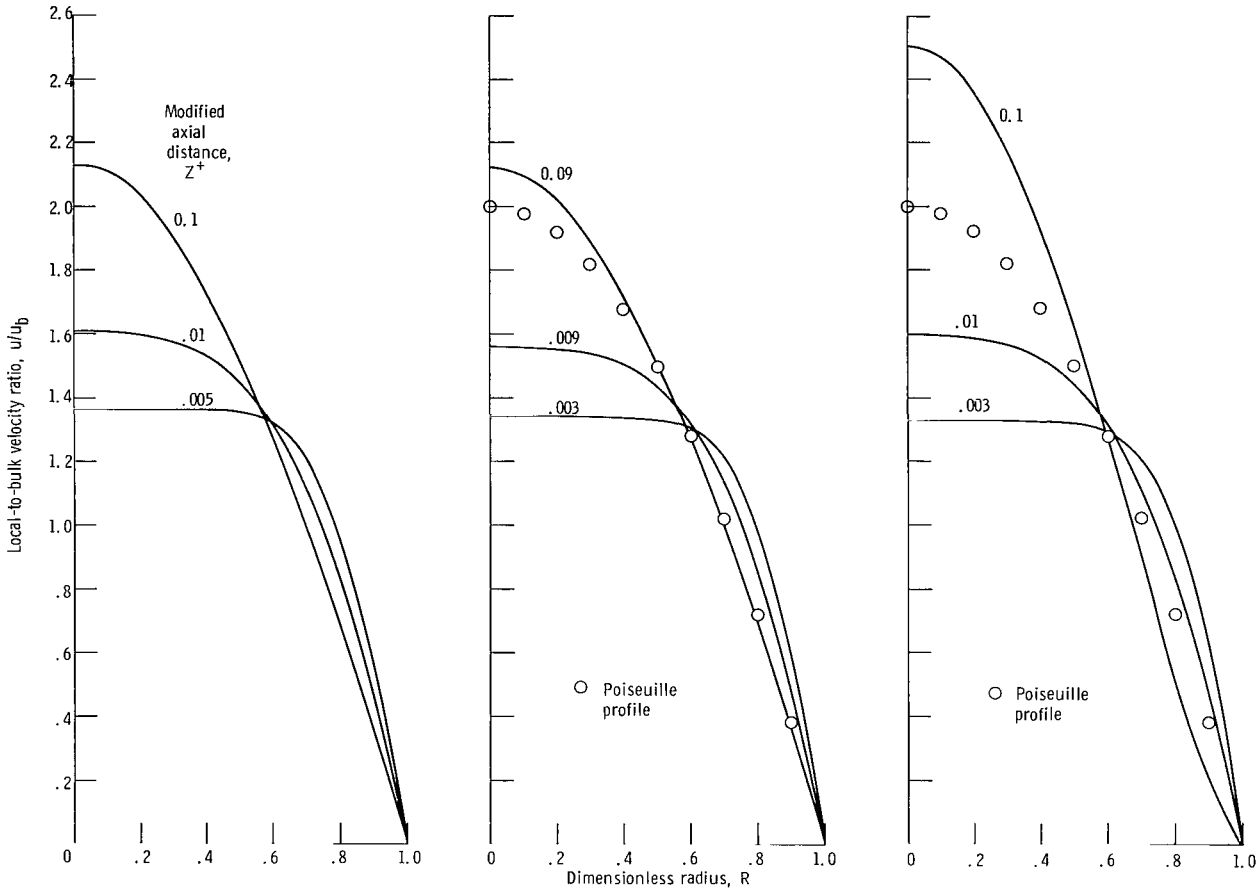

(c) Initial Mach number, 0.004; dimensionless cooling flux parameter, -1.35 (high cooling flux).

(d) Initial Mach number, 0.06; dimensionless cooling flux parameter, -1.35 (high heat flux).

(e) Initial Mach number, 0.30; dimensionless cooling flux parameter, -1.35 (high cooling flux).

Figure 2. - Concluded.

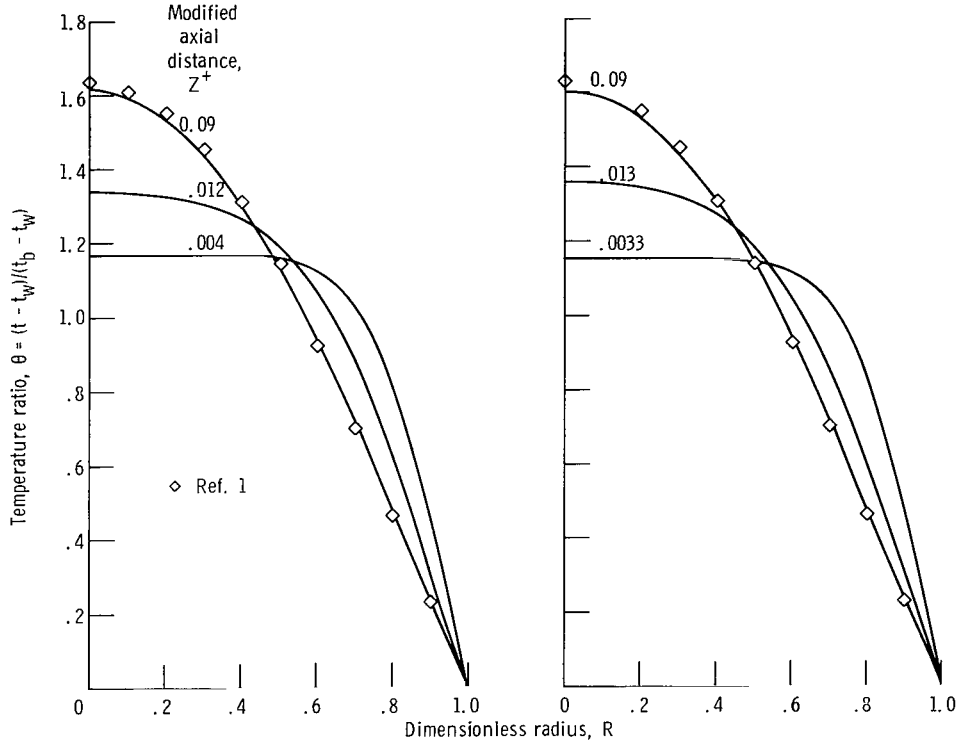

(a) Initial Mach number, 0.004; dimensionless cooling flux parameter, -0.135 (low cooling flux).

(b) Initial Mach number, 0.06; dimensionless cooling flux parameter, -0.135 (low cooling flux).

Figure 3. - Developing static temperature profiles across tube radius.

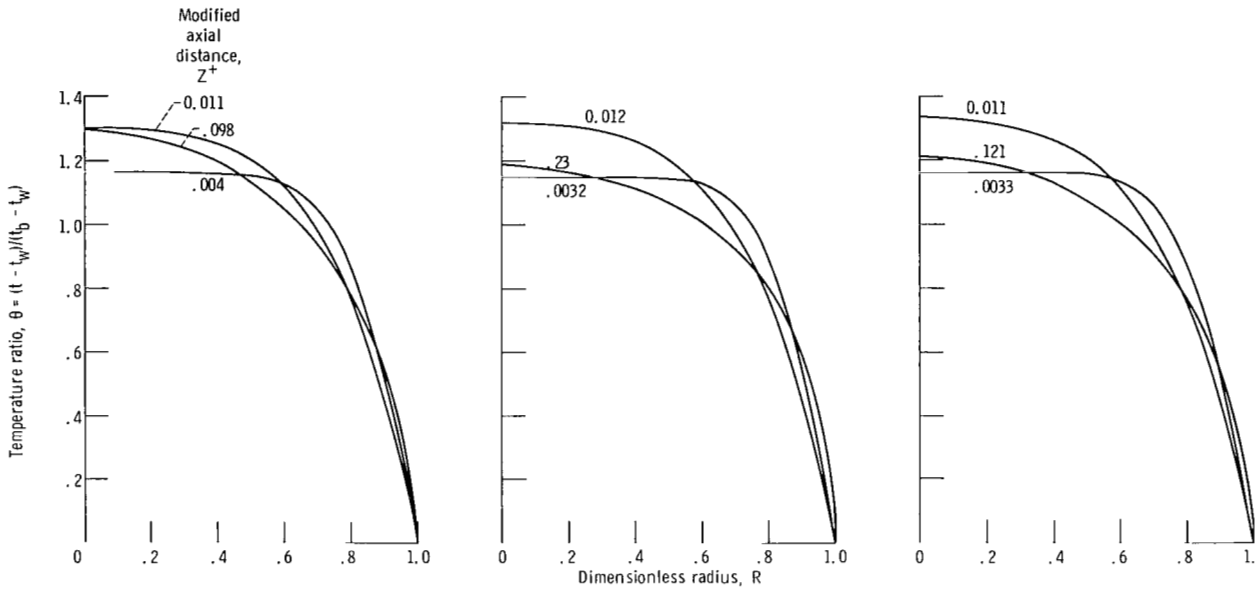

(c) Initial Mach number, 0.004; dimensionless cooling flux parameter, -1.35 (high cooling flux).

(d) Initial Mach number, 0.06; dimensionless cooling flux parameter, -1.351 (high cooling flux).

(e) Initial Mach number, 0.30; dimensionless cooling flux parameter, -1.35 (high cooling flux).

Figure 3. - Concluded.

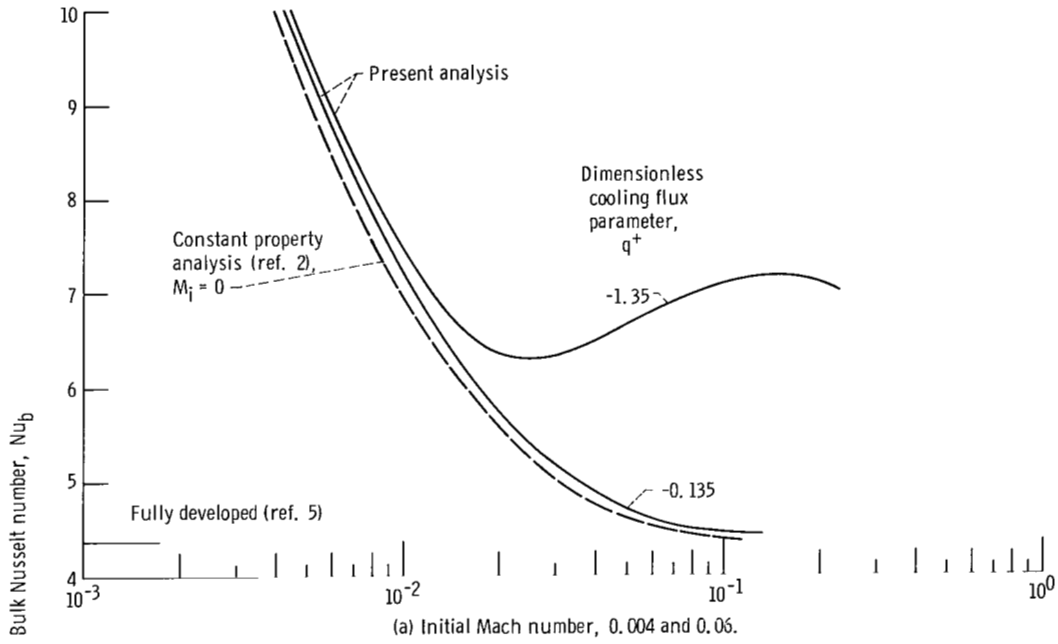

(a) Initial Mach number, 0.004 and 0.06.

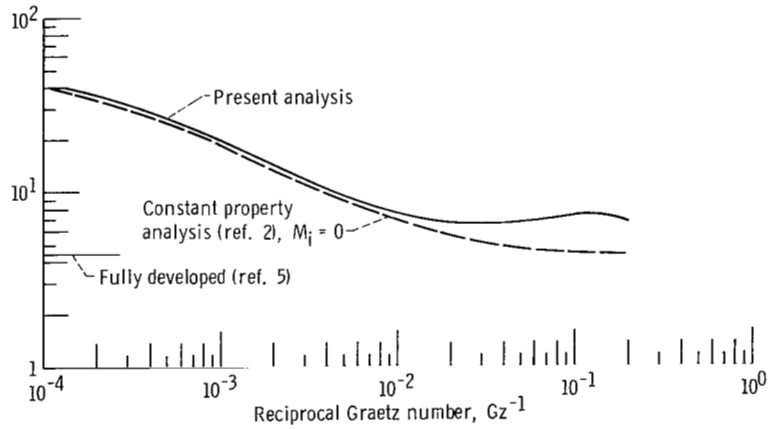

(b) Initial Mach number, 0.30; dimensionless cooling flux parameter, -1.35 (high cooling flux).

Figure 4. - Local Nusselt numbers plotted against dimensionless distance from tube entrance.

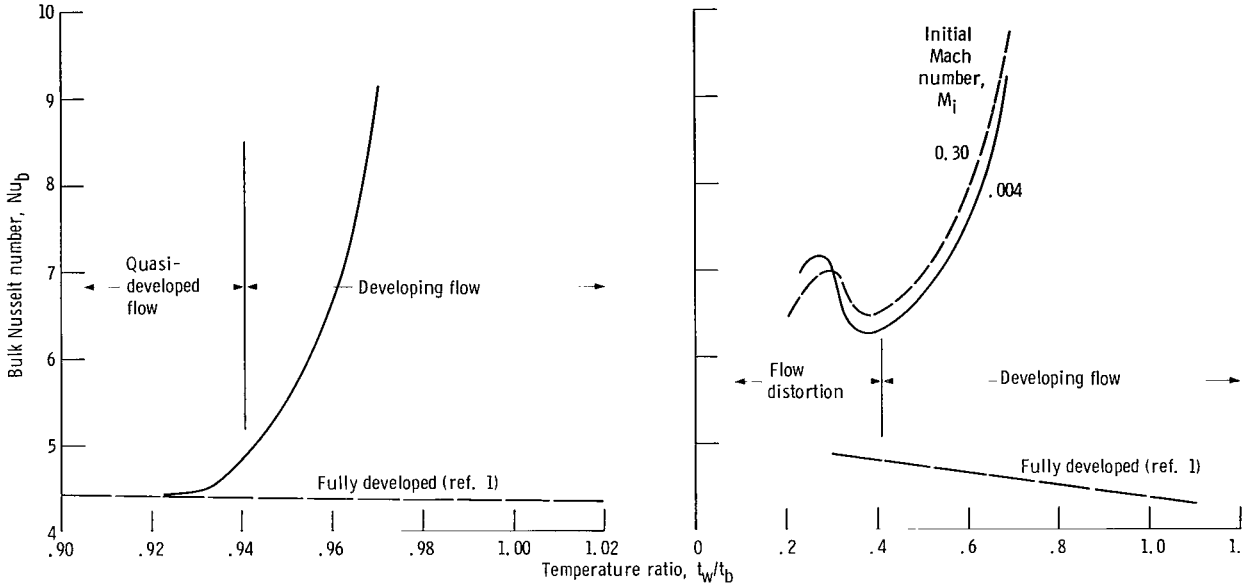

(a) Initial Mach number, 0.004; dimensionless cooling flux, -0.135 (low cooling flux).

(b) Dimensionless cooling flux parameter, -1.35 (high cooling flux).

Figure 5. - Comparison of developing local Nusselt numbers with values from analysis of fully developed flow with property variation.

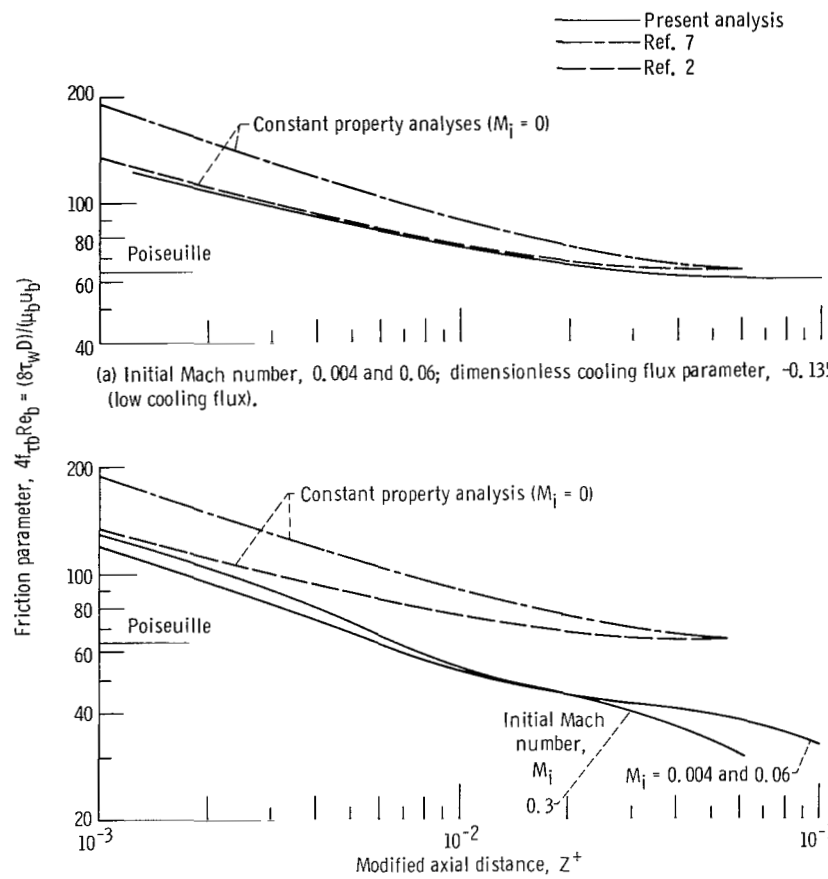

(a) Initial Mach number, 0.004 and 0.06; dimensionless cooling flux parameter, -0.135 (low cooling flux).

(b) Dimensionless cooling flux parameter, -1.351 high cooling flux).

Figure 6. - Friction parameter based on local shear stress plotted against dimensionless distance from tube entrance.

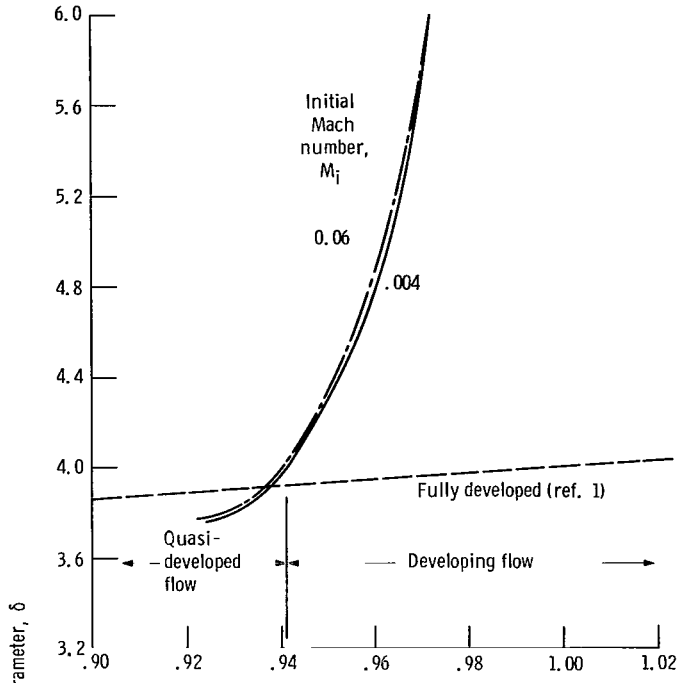

(a) Dimensionless cooling flux parameter, -0.135 (low cooling flux).

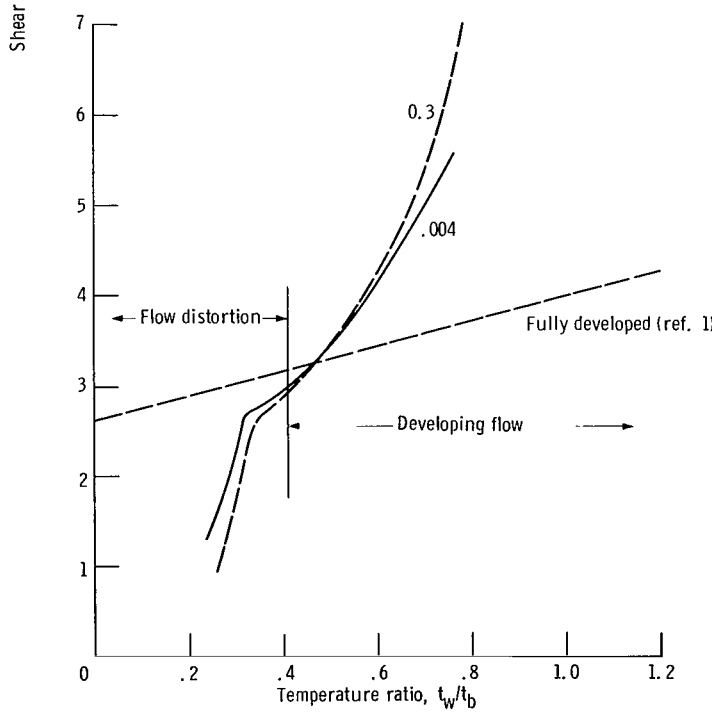

(b) Dimensionless cooling flux parameter, -1.35 (high cooling flux.

Figure 7. - Comparison of developing local shear stress parameter with values from analysis of fully developed flow with property variation.

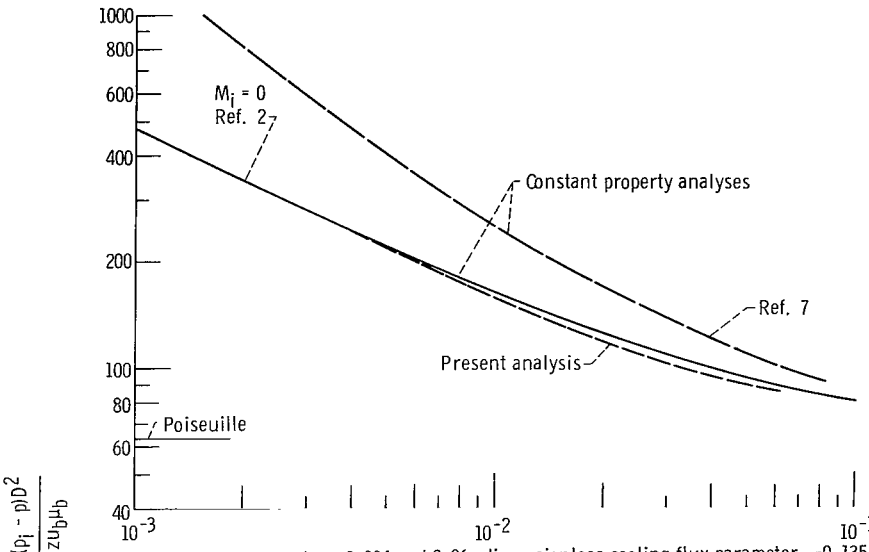

(a) Initial Mach number, 0.004 and 0.06; dimensionless cooling flux parameter, -0.135 (low cooling flux).

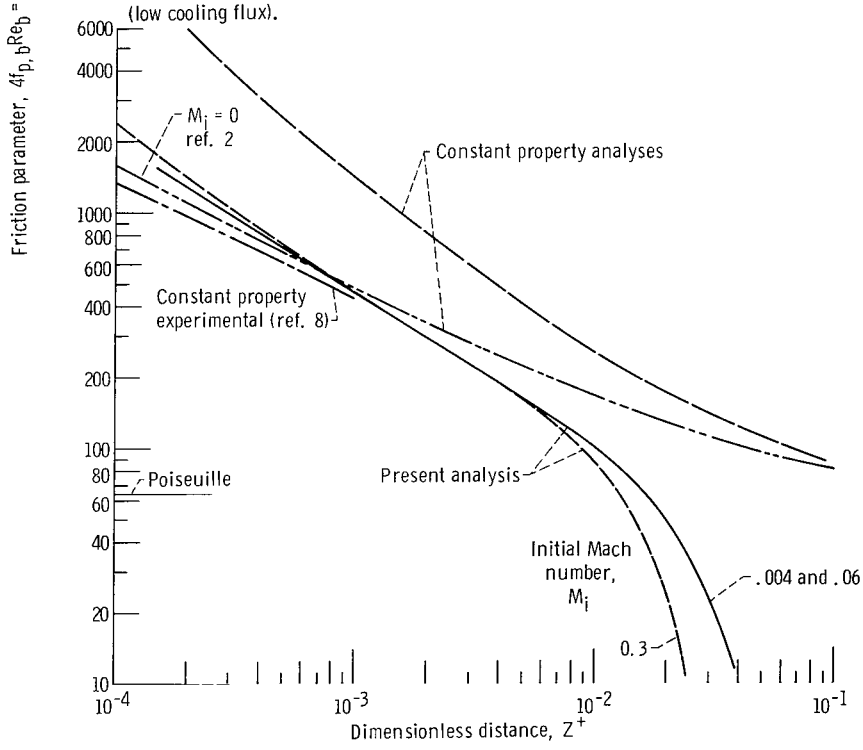

(b) Dimensionless cooling flux parameter, -1.35 (high cooling flux).

Figure 8. - Average friction factor based on static pressure drop plotted against dimensionless distance from tube entrance.

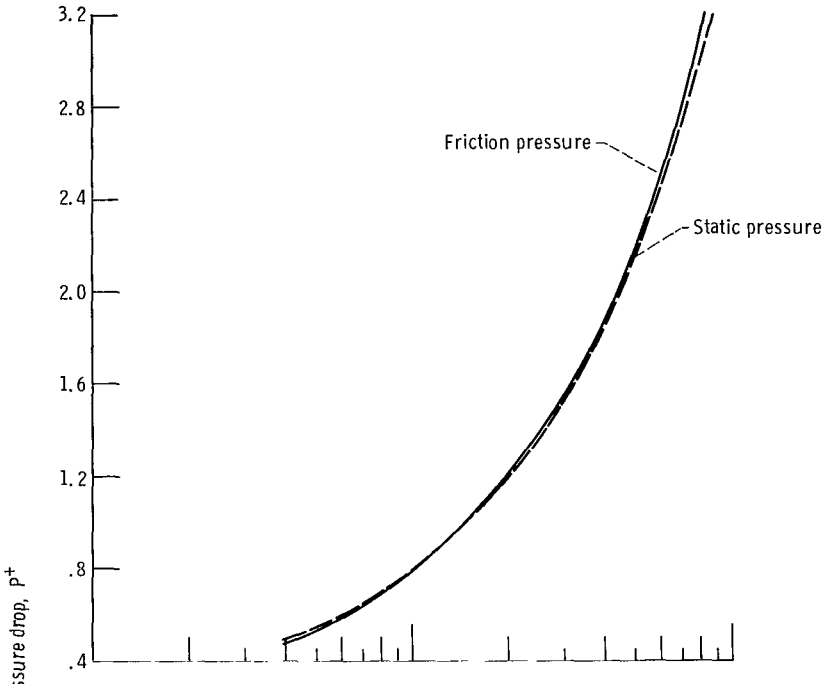

(a) Initial Mach number, 0.004; dimensionless cooling flux parameter, -0.135 (low cooling flux).

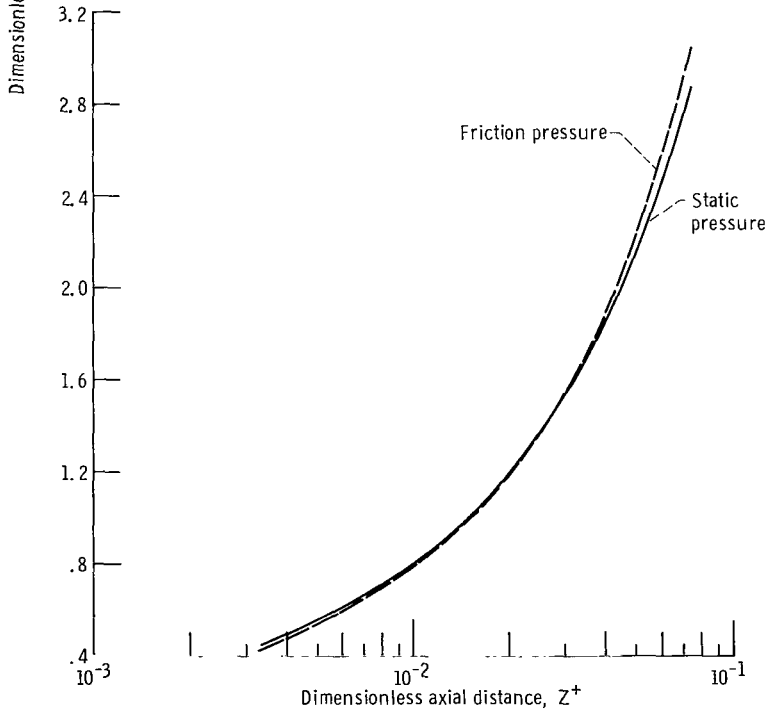

(b) Initial Mach number, 0.06; dimensionless cooling flux parameter, -0.135 (low cooling flux).

Figure 9. - Static and frictional pressure drop in entrance length of tube with cooling.

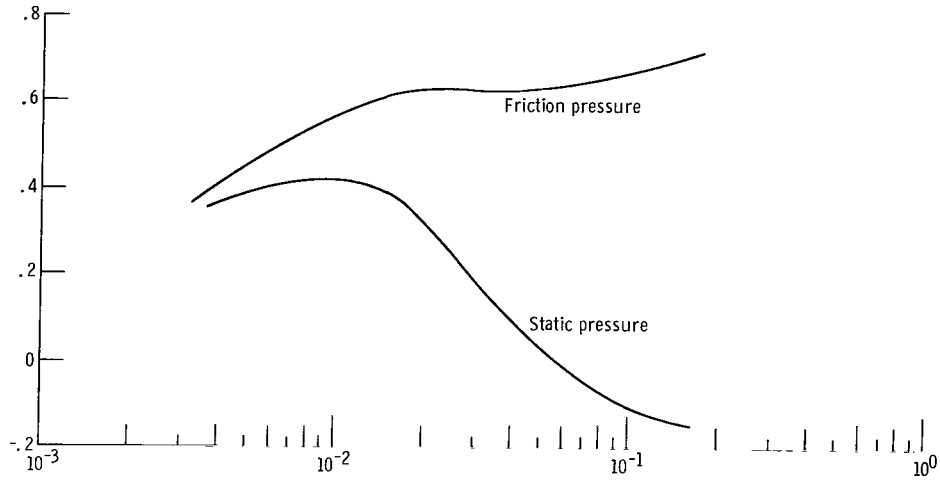

(c) Initial Mach number, 0.004; dimensionless cooling flux parameter, -1.35 (high cooling flux).

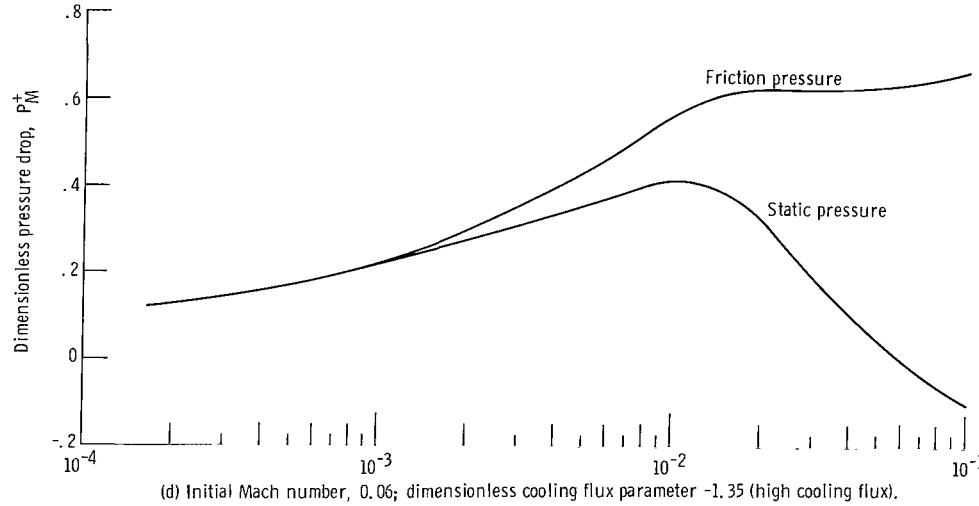

(d) Initial Mach number, 0.06; dimensionless cooling flux parameter -1.35 (high cooling flux).

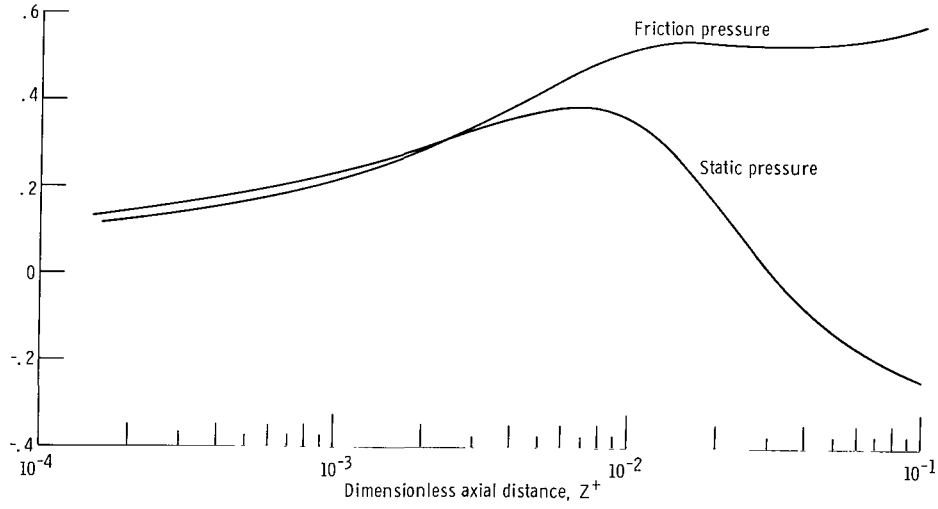

(e) Initial Mach number, 0.3; dimensionless cooling flux parameter, -1.35 (high cooling flux).

Figure 9. - Concluded.

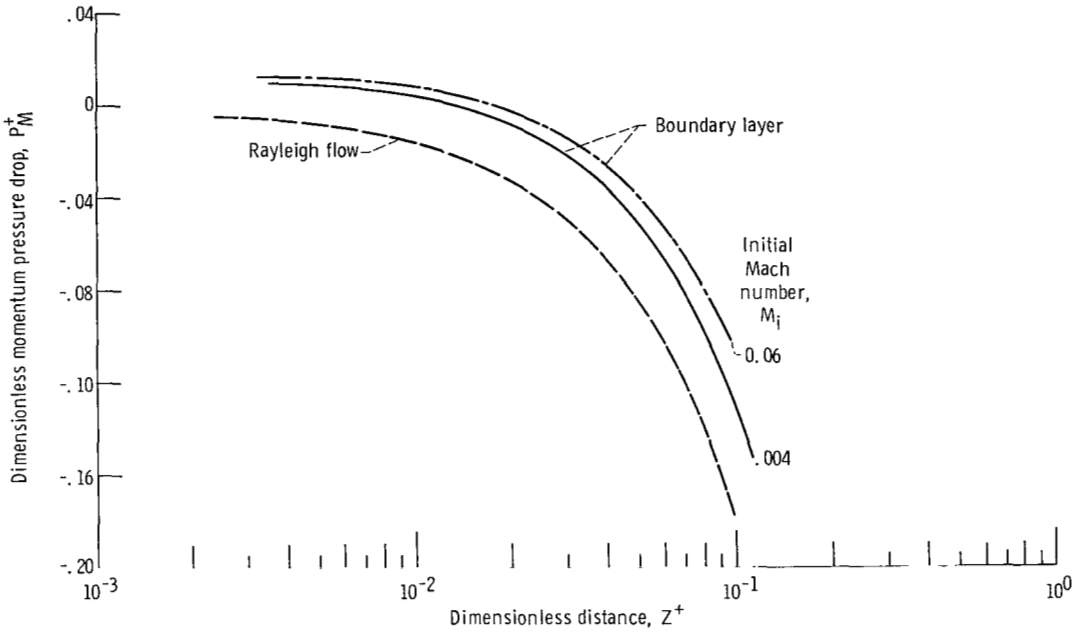

(a) Dimensionless cooling flux parameter, -0.135.

Figure 10. - Momentum pressure change by boundary layer calculation and Rayleigh flow (cooling).

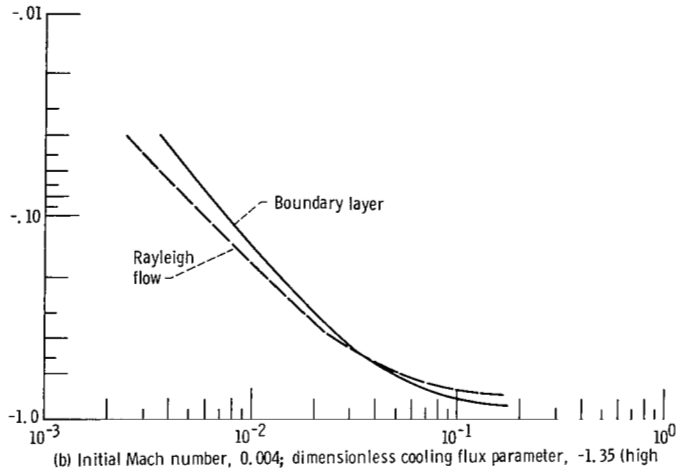

(b) Initial Mach number, 0.004; dimensionless cooling flux parameter, -1.35 (high cooling flux).

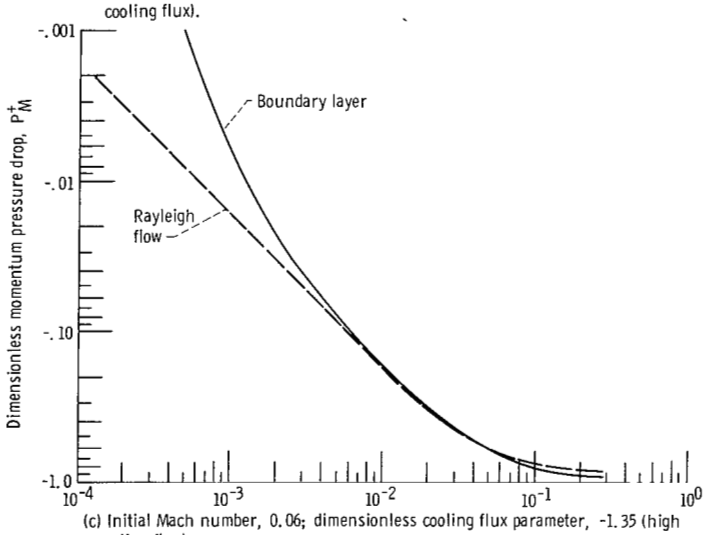

(c) Initial Mach number, 0.06; dimensionless cooling flux parameter, -1.35 (high cooling flux).

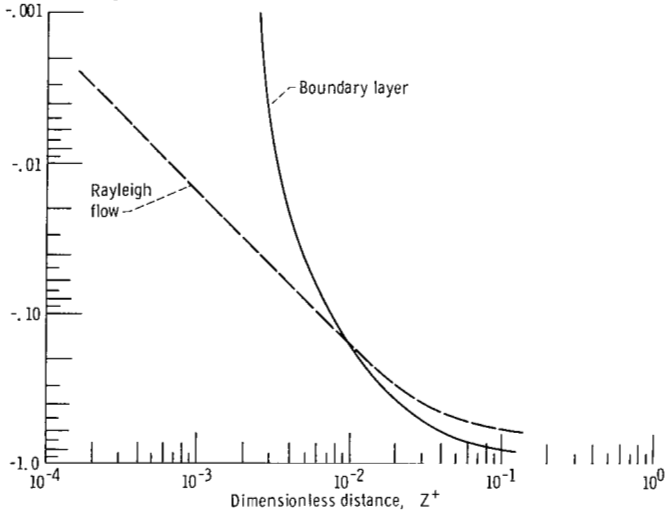

(d) Initial Mach number, 0.3; dimensionless cooling flux parameter, -1.35 (high cooling flux).

Figure 10. - Concluded.

NASA-Langley, 1971 —— 12 E-5606

"The aeronautical and space activities of the United States shall be conducted so as to contribute . . . to the expansion of human knowledge of phenomena in the atmosphere and space. The Administration shall provide for the widest practicable and appropriate dissemination of information concerning its activities and the results thereof."

— NATIONAL AERONAUTICS AND SPACE ACT OF 1958

NASA SCIENTIFIC AND TECHNICAL PUBLICATIONS

TECHNICAL REPORTS: Scientific and technical information considered important, complete, and a lasting contribution to existing knowledge.

TECHNICAL NOTES: Information less broad in scope but nevertheless of importance as a contribution to existing knowledge.

TECHNICAL MEMORANDUMS: Information receiving limited distribution because of preliminary data, security classification, or other reasons.

CONTRACTOR REPORTS: Scientific and technical information generated under a NASA contract or grant and considered an important contribution to existing knowledge.

TECHNICAL TRANSLATIONS: Information published in a foreign language considered to merit NASA distribution in English.

SPECIAL PUBLICATIONS: Information derived from or of value to NASA activities. Publications include conference proceedings, monographs, data compilations, handbooks, sourcebooks, and special bibliographies.

TECHNOLOGY UTILIZATION PUBLICATIONS: Information on technology used by NASA that may be of particular interest in commercial and other non-aerospace applications. Publications include Tech Briefs, Technology Utilization Reports and Technology Surveys.

Details on the availability of these publications may be obtained from:

SCIENTIFIC AND TECHNICAL INFORMATION OFFICE

NATIONAL AERONAUTICS AND SPACE ADMINISTRATION

Washington, D.C. 20546